Supporting Information
Few-hundred GHz Carbon Nanotube NEMS

J. O. Island, V. Tayari, A. C. McRae, and A. R. Champagne*
Department of Physics, Concordia University, Montréal, Québec, H4B 1R6, Canada
*E-mail: a.champagne@concordia.ca

Supporting information contents

1. Transport data for Devices D and E

We measured *dI/dV*-V_B-V_G data for two additional ultra-short quantum dot SWCNT NEMS. The data for these devices are shown in Fig. S1a-b for Devices D and E respectively. The geometry of these devices and their single-electron transport characteristics were described in detail in a previous publication[1], and reveal tube lengths of $\approx 10\,nm$. The black arrows in Fig. S1 indicate the position of stretching mode resonances.

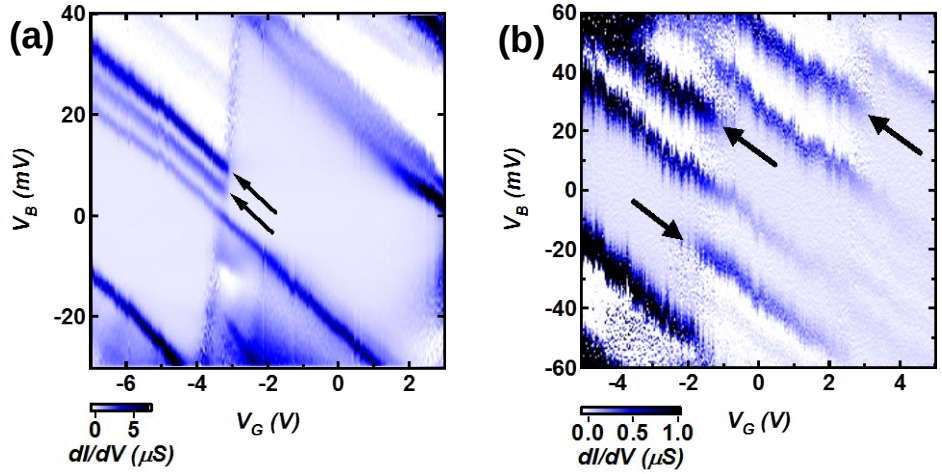

Figure S1: *dI/dV*-V_B-V_G data for (a) ultra-short Device D and (b) ultra-short Device E, showing the presence of stretching mode vibrons (arrows), but no bending mode resonance.

However, no bending mode resonance is observed. The range of current we explored in Devices D and E only marginally approached the anticipated location of the bending resonance, $I \approx ef_{bend}$, which may explain its absence. Another possibility to explain the absence of bending mode in D and E is a smaller *e-v*$_{bend}$ coupling than in Devices A, B, C, as the coupling is expected to scale with the length of the NEMS[2].

2. Tension from the electrostatic bending of the suspended bow-tie contacts

This section first presents the details of the suspended bow-tie (breakjunction) contact geometry of Devices A, B, D and E. We then calculate a theoretical estimate of the strain and tension applied to the nanotube NEMS when a gate voltage is used to controllably bend down the suspended bow-tie contacts, both in the regime of low tension (loose tube) and high tension (tight tube).

Figure S2 shows the bow-tie geometry. Panel (a) is a top view SEM of Device A before electromigration (continuous gold bridge). The breakjunction is approximately 350 nm wide at its center, 700 nm at its base, and 925 nm long. Using a controlled electromigration technique, we create a gap in the gold bridge and expose the nanotube which lies directly underneath the junction[1]. Fig. S2b is a tilted view ($\approx 75°$) of Device E after electromigration, where we can see the suspended gold bridge above the substrate, and the break in the center of the bridge. The result is two gold cantilever beam contacts connecting to a suspended SWCNT as in Fig. 1a. We also notice in Fig. S2b that the silicon oxide etch reached underneath the wide gold bars anchoring the bridge, creating an "undercut".

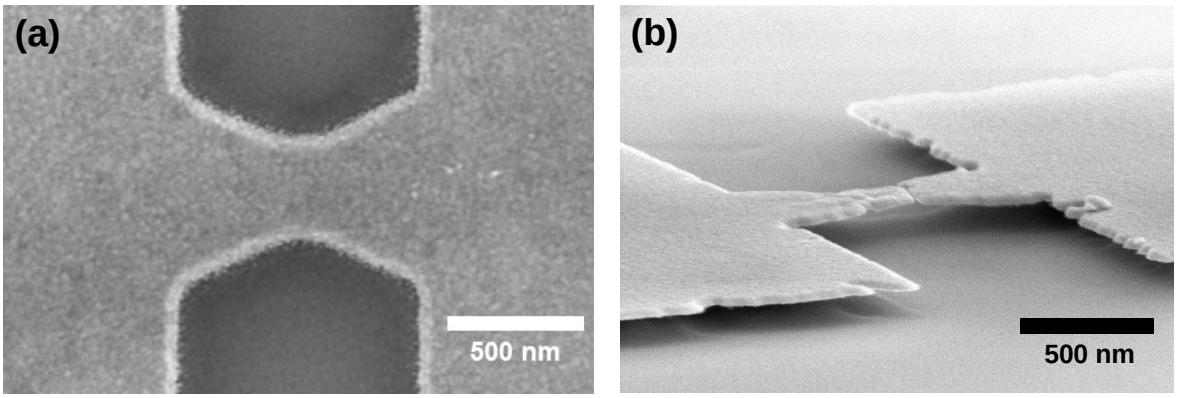

Figure S2: (a) SEM image of Device A before electromigration showing a constriction width of $\approx 350\,nm$. (b) Titled SEM image of Device E showing the suspended breakjunction after electromigration.

We apply a voltage V_G to the gate electrode to create an electrostatic force between the gate (substrate) and the two gold cantilevers, pulling them down to apply a tension/strain to the short nanotube. The cantilevers act as lever arms which enable us to apply large strains to the SWCNT-NEMS. The electrostatic force between the two plates of a parallel plate capacitor is $F = \frac{1}{2}\frac{CV_G^2}{t}$, where C is the capacitance, V_G is the

gate voltage, and t is the spacing between the two plates. For our devices, the capacitance can be modeled by two capacitors in series, respectively with a vacuum dielectric of thickness t_{vac} and a SiO_2 dielectric of thickness t_{ox}. We label the areas of the two gold cantilevers, A_{lc} and A_{rc} respectively for the left and right cantilever, and find for the expression for the electrostatic force on the left cantilever to be,

$$F_{lc} = \frac{\varepsilon_{vac} A_{lc}}{2}\left[\frac{(\varepsilon_{ox}/\varepsilon_{vac})V_g}{t_{ox} + (\varepsilon_{ox}/\varepsilon_{vac})t_{vac}}\right]^2 \quad (1)$$

where $\varepsilon_{ox} = 3.9\varepsilon_{vac}$, and ε_{vac} is the permittivity of free space. To estimate the displacement of the cantilever due to this electrostatic force, we model it as a rectangular beam with a uniformly distributed load. The vertical displacement (bending), $\Delta y_{lc}(x)$, along the beam is

$$\Delta y_{lc}(x) = \frac{F_{lc}x^2}{2L_{lc}Y_{Au}wt_{Au}^3}(x^2 + 6L_{lc}^2 - 4L_{lc}x) \quad (2)$$

Where x is the position along the beam, $Y_{Au} = 60\ GPa$ is the Young's modulus for e-beam evaporated gold thin films[3], $t_{Au} = 40\ nm$ is the cantilever thickness, w is the average width of the cantilever, and L_{lc} is the cantilever's length. We can define an effective spring constant, k_{lc}, for this cantilever using $\Delta y_{lc}(L_{lc}) = F_{lc}/k_{lc}$,

$$k_{lc} = \frac{2}{3}\frac{Y_{Au}w{t_{Au}}^3}{{L_{lc}}^3} \quad (3)$$

From geometry, we calculate the elongation (strain) of the tube between the two bent cantilevers to be

$$\frac{\Delta L_{tube}}{L_{tube}} = \frac{1}{L_{tube}}\left\{\left[\left(L_{tube} + L_{lc} - \sqrt{L_{lc}^2 - (\Delta y_{lc})^2} + L_{rc} - \sqrt{L_{rc}^2 - (\Delta y_{rc})^2}\right)^2 + (\Delta y_{lc} - \Delta y_{rc})^2\right]^{1/2} - L_{tube}\right\} \quad (4)$$

Then the tension, *T,* is

$$T = \left(\frac{\Delta L_{tube}}{L_{tube}}\right) Y_{tube} * 2\pi r * 0.335\ nm \quad (5)$$

where Y_{tube} = 1 TPa, and *r* = 1 ± 0.3 nm is the radius of our tubes, and 0.335 nm is the thickness of graphene.

From *Sapmaz et al.*[4] the fundamental bending frequency of SWCNTs as a function of tension is respectively for the low and high tension regime:

$$f_{low} = \frac{r}{4\pi}\sqrt{\frac{Y_{tube}}{\rho}}\left\{\frac{22.38}{{L_{tube}}^2} + \frac{0.3565}{r^4}\frac{T}{Y_{tube}}\right\} \quad when\ \frac{2L_{tube}}{\sqrt{\pi}r^2}\sqrt{\frac{T}{Y_{tube}}} \ll 1 \quad (6)$$

$$f_{high} = \frac{1}{2\pi}\left[\frac{1.77}{L_{tube}\,r}\sqrt{\frac{T}{\rho}} + \frac{\pi r}{{L_{tube}}^2}\sqrt{\frac{Y_{tube}}{\rho}}\right] \quad when\ \frac{2L_{tube}}{\sqrt{\pi}r^2}\sqrt{\frac{T}{Y_{tube}}} \gg 1 \quad (7)$$

We now use the above expressions to calculate the tension and frequency of Device A as a function of V_G. Figure S3a is a tilted SEM image of Device A. It shows no significant bending of the cantilever contacts, and that the cantilevers are suspended above the substrate. The thickness of the vacuum gap between the gold cantilevers and the substrate can be estimated to be roughly equal to the thickness of the gold film (40 nm). A more precise measurement of this distance is shown in Fig. 3b-c where respectively 2D and 1D AFM scans are shown (1D scan is along the white line (b)). The average vertical height of the cantilever beams from these images is 75 ± 5 nm. After subtracting the thickness of the gold film (40 nm), we measure t_{vac} = 35 ± 5 nm. The same t_{vac} is measured across the two cantilever beams. The thickness of SiO_2 is t_{ox} = 100 nm (measured by ellipsometry). We measure the cantilever lengths to be L_{lc} = 550 + 500 = 1050 nm, and L_{rc} = 330 + 500 = 830 nm, where 500 nm is the approximate length (from AFM imaging) of the etch undercut under the gold contacts which adds to the length of the suspended lever arms. The average width of the cantilever beams is $w_{average} \approx 525\,nm$, the areas under the beams are approximated as $A_{lc} = w_{average} \times L_{lc} = 5.5 \times 10^5\,nm^2$, $A_{rc} = w_{average} \times L_{rc} = 4.4 \times 10^5\,nm^2$, the length of the SWCNT is $L_{tube} = L_G = 27\,nm$ (Device A), and ρ = 870 kg/m^3 is the mass density of the tube.

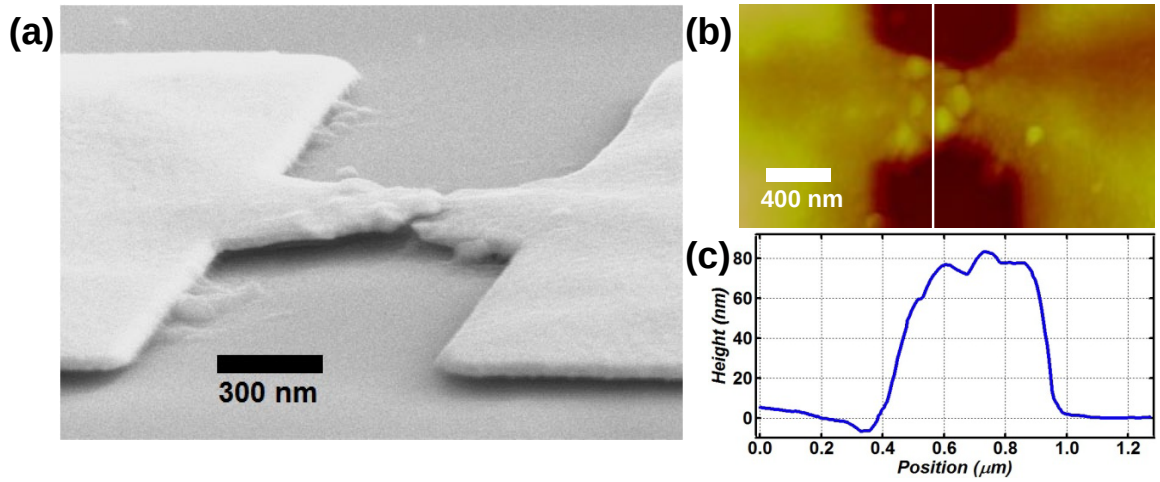

Figure S3: (a) Tilted SEM image of Device A taken at an angle of 70°. (b) 2D AFM scan of Device A. The full color scale is 200 nm, and the white line shows the position of the 1D height scan in (c). The AFM scans show a suspended height of 35 ± 5 nm for the bridge, after subtracting the thickness of the gold film (40 nm).

To calculate F_{lc} and k_{lc} using Eqs. 1 and 3, we need to estimate t_{vac} when $V_G \neq 0$. As the gold cantilever bends, $t_{vac}(x) = 35\,nm - \Delta y(x)$ varies along the length of the beam. Since the exact displacement of the beam depends on many microscopic details, our aim is to calculate a reasonable estimate for the displacement, and verify that it is consistent with the tension inferred from our transport measurements of f_{bend}. Integrating Eq. 2, we find the average vertical displacement along the beam $\Delta y_{lc-avg} = \frac{2}{5}\Delta y_{lc}(L)$. Thus we let $t_{vac} = t_{vac-avg} = 35\,nm - \frac{2}{5}\Delta y_{lc}(L)$ in Eq. 1, and similarly for the right cantilever.

Using Eqs. 1-7, we find for Device A that the mid-point between the low and high tension regime is around $T = 1.1 \times 10^{-9}\, N$ and corresponds to $V_G \approx 1.5\, V$. We solve numerically for the frequencies in the low and high tension regimes and find

$$f_{low} = 8.28 \times 10^{10} Hz + 7.50 \times 10^{10} \times \left\{ \left[\left(27 + 1050 - \sqrt{(1050)^2 - (0.572 V_G^2)^2} \right)^2 + (0.572 V_G^2 - 0.223 V_G^2)^2 \right]^{1/2} - 27 \right\} Hz \quad (8)$$

$$f_{high} = 2.33 \times 10^{10}\, Hz + 9.88 \times 10^{10} \times \left\{ \left[\left(27 + 1050 - \sqrt{(1050)^2 - \left((0.6694 - 0.0680|V_G| + 0.0164 V_G^2) V_G^2 \right)^2} \right)^2 + \left(830 - \sqrt{(830)^2 - \left((0.2118 + 0.0057|V_G|) V_G^2 \right)^2} \right)^2 + \left((0.6694 - 0.0680|V_G| + 0.0164 V_G^2) V_G^2 - (0.2118 + 0.0057|V_G|) V_G^2 \right)^2 \right]^{1/2} - 27 \right\}^{1/2} Hz \quad (9)$$

The current $I = e f_{bend}$ for these two regimes is plotted in Fig. 4b of the main text. f_{bend} is almost constant around 83 GHz at low tension, and closely matches the measured current at low V_G. At high V_G, the calculated f_{bend} agrees qualitatively with the current minima (Coulomb valleys) and quantitatively for the valley around $V_G \approx$ -4.2 V which is one of the best resolved Coulomb valley in Fig. 4a. This is where we expect the $I \approx e f_{bend}$ relation to hold, since in this region the only tunneling events allowed involve bending vibrons. The measured I = 24 nA at V_G = -4.2 V , corresponds to $f_{bend} \approx$ 150 GHz, while using Eq. 9 we calculate f_{bend} = 129 GHz. The agreement between the data and calculation indicates that we can tune f_{bend} by close to a factor of two by varying V_G from 0 to - 4.2 V. The tube's strain for Device A, according to both the estimate of the gold cantilever motion (Eq. 9), and extracted from the data using Eq. 7 are respectively 4.4 % and 6.0 %.

The gold bridge in Device B was fabricated with dimensions identical to those of Device A. Device B was damaged after the transport measurements were completed, and a SEM image of this device is not available. However, the Coulomb transport data for Device B confirms that the dimensions of the device L_{tube}, t_{vac} are very close to those of Device A. Thus we expect the tension and strain versus V_G in Device B to be of the same order of magnitude as in Device A.

Device C, shown in Fig. 1b and S5a, does not have long bow-tie cantilever contacts. The length of the suspended portion of the contacts in Device C is only $\approx 270\, nm$ (etch undercut), and from Eq. 3, $k_{lc} \propto \frac{1}{{L_{lc}}^3}$, the tension induced by V_G is negligible in Device C. The dominant source of tension in Device C comes from the permanent bending of its electrodes (section 5) which occurred during the suspension process.

3. Gate capacitance model

The gate capacitance for a nanotube transistor can be modeled as a wire over a metallic plane (doped-Si wafer) separated by an insulator (vacuum or oxide), giving[5]

$$\frac{C_G}{L_G} = \frac{2\pi\varepsilon}{\cosh^{-1}\left(\frac{t}{r}\right)} \tag{10}$$

where, ε is the permittivity of the insulator, L_G is the tube length, t is thickness of the insulator, and r is the radius of the nanotube. After a BOE acid etch, the tube is suspended and separated from the gate by layers of vacuum and SiO_2 in series. We extend the above model to combine these two capacitors in series,

$$\frac{C_G}{L_G} = \frac{2\pi\varepsilon_{ox}}{\frac{\varepsilon_{ox}}{\varepsilon_{vac}} * \cosh^{-1}\left(\frac{t_{vac}}{r}\right) + \cosh^{-1}\left(\frac{t_{vac}+t_{ox}}{r+t_{vac}}\right)} \tag{11}$$

where ε_{ox} and ε_{vac} are the permittivity constants of SiO_2 and vacuum respectively, and t_{ox} and t_{vac} are the oxide and vacuum layer thicknesses. Using Eq. 11, we calculate L_G with the gate capacitance extracted from the width of the Coulomb diamonds.

We find that, Device A ($t_{ox} = 100\,nm$, $t_{vac} = 35\,nm$, $r = 1 \pm 0.3\,nm$) has a tube length of $L_G = 27 \pm 4\,nm$, Device B ($t_{ox} = 100\,nm$, $t_{vac} = 35\,nm$, $r = 1 \pm 0.3\,nm$) has a tube length of $L_G = 30 \pm 4\,nm$, and Device C ($t_{ox} = 115\,nm$, $t_{vac} = 115\,nm$, $r = 1 \pm 0.3\,nm$) has a tube length of $L_G = 23 \pm 4\,nm$.

4. Additional data for Device B

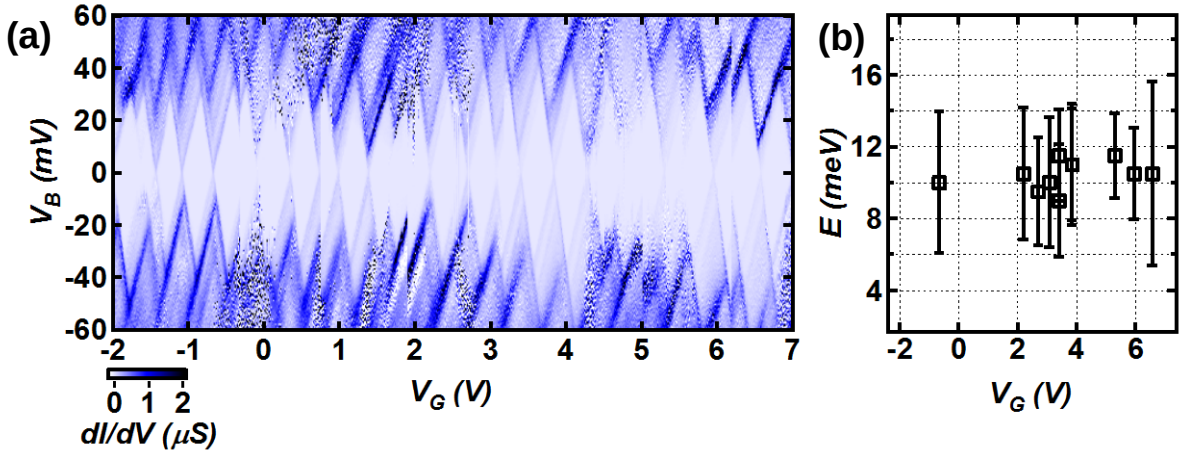

Figure S4: Additional data for Device B. (a) 2D dI/dV-V_B-V_G data (b) The vibron energies measured in (a) show no clear change as a function of the tension applied by the suspended breakjunction as V_G increases, as expected for stretching modes.

Figure S4a shows the transport data over a broad range of V_G for Device B. The energies of the lowest stretching mode vibron resonances in each of the Coulomb diamonds were extracted from this data, and are shown in Fig. S4b.

5. Built-in tension in Device C

Figure S5a shows a titled (60^o) SEM image of Device C. We use this image to measure the dimensions and angles defined in Fig. S5b, and calculate the SWCNT strain due to the permanent contact bending,

$$\frac{\Delta L}{L} = \frac{\sqrt{[L + e_1(1 - cos\theta_1') + e_2(1 - cos\theta_2')]^2 + (Lsin\phi')^2} - L}{L} \qquad (12)$$

Where the angles $\theta'_1, \theta'_2, \phi'$ refer to the angles shown in Fig. S5b, while the angles θ_1, θ_2, ϕ are the angles measured in Fig. S5a. They differ due to the tilting of the SEM image, $\alpha = 60°$, and $\theta' = \tan^{-1}\left(\frac{\tan\theta}{\sin\alpha}\right)$. Using Eq. 12, and the measured parameters for Device C: $e_1 = 270\ nm$, $e_2 = 270\ nm$, $L = 78\ nm$, $\theta_1' = 0°$,$\theta_2' = 7°$, $\phi' = 23°$, we obtain a strain of $\Delta L/L = 0.098$.

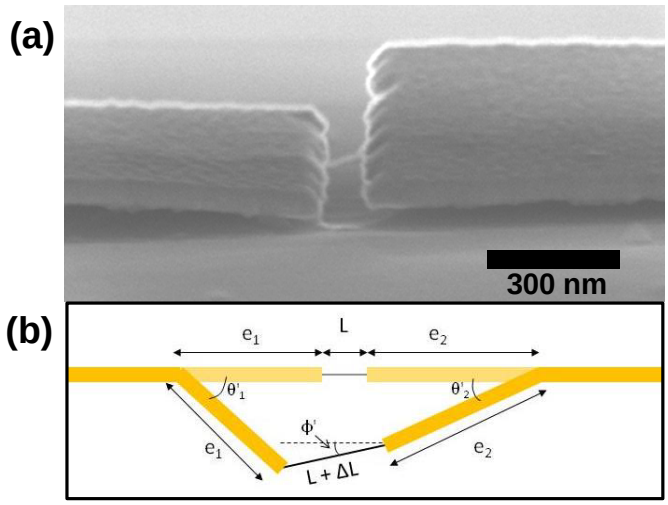

Figure S5: Static (built-in) strain for Device C. (a) Tilted-view SEM image of Device C taken at an angle of $60°$. (b) Parameters used in Eq. 12 to calculate the built-in strain.

6. Q-factor calculations

The quality factor for a SWCNT-NEMS is calculated from the energy lost during one oscillation cycle and was derived by *Lassagne et al.* [6],

$$\frac{1}{Q} = \frac{2\pi f_{bend}}{k_{tube}}\left(\frac{2C'_G V_G}{\Gamma C_\Sigma}\right)^2 G \qquad (13)$$

where, k_{tube} is the spring constant of the suspended nanotube, C'_G is the derivative of the gate capacitance with respect to t_{vac} (vertical displacement), V_G is the gate voltage, Γ is the tunneling rate, $C_\Sigma = C_{source} + C_{drain} + C_{gate}$ is the total quantum dot capacitance,

and G is the conductance. The spring constant is estimated from the equation for simple harmonic motion,

$$k_{tube} = m_{eff}(2\pi f_{bend})^2 \qquad (14)$$

where $m_{eff} = 0.735 * m = 0.735\rho L\pi r^2$ is the effective mass of a doubly clamped cylindrical beam oscillator. For our nanotubes, the mass density is $\rho = 870\ kg/m^3$ and the tube radius is $r = 1 \pm 0.3\ nm$. Using Eq. 11 above, we calculate C'_G as

$$\frac{dC_G}{dt_{vac}} = -\frac{2\pi\varepsilon_{ox}L_G}{\left(\frac{\varepsilon_{ox}}{\varepsilon_{vac}}\cosh^{-1}\left(\frac{t_{vac}}{r}\right) + \cosh^{-1}\left(\frac{t_{vac}+t_{ox}}{r+t_{vac}}\right)\right)^2}\left[\frac{\frac{\varepsilon_{ox}}{\varepsilon_{vac}}}{r\sqrt{\left(\frac{t_{vac}}{r}\right)^2 - 1}}\right. \qquad (15)$$
$$\left. + \frac{1}{\sqrt{\left(\frac{t_{vac}+t_{ox}}{r+t_{vac}}\right)^2 - 1}}\left(\frac{1}{t_{vac}+r} - \frac{t_{vac}+t_{ox}}{(t_{vac}+r)^2}\right)\right]$$

where L_G is the tube length, ε_{ox} and ε_{vac} are the permittivity constants of SiO_2 and vacuum respectively, and t_{ox} and t_{vac} are the oxide and vacuum layers thicknesses.

We use Eqs. 13-15 for Device A with the following parameters: $t_{vac} = 35\ nm$, $t_{ox} = 100\ nm$, $L = 27\ nm$, $r = 1\ nm$, $C'_G = -1.25 * 10^{-12} F/m$, $m_{eff} = 4.4 * 10^{-23} kg$, $f_{bend} = 75\ GHz$, $k = 9.8\ N/m$, $V_G = -0.55\ V$, $\Gamma = 75\ \mathrm{GHz}$, $C_\Sigma = 3.8 * 10^{-18} F$, $G = 3.1 * 10^{-7}\ S$, and calculate a quality factor of $Q = 2.9 * 10^6$.

We use Eqs. 13-15 for Device C with the following parameters: $t_{vac} = 115\ nm$, $t_{ox} = 115\ nm$, $L = 23\ nm$, $r = 1\ nm$, $C'_G = -9.9 * 10^{-13} F/m$, $m_{eff} = 4.6 * 10^{-23} kg$, $f_{bend} = 280\ GHz$, $k = 1.45 * 10^2\ N/m$, $V_G = -3.9\ V$, $\Gamma = 280\ \mathrm{GHz}$, $C_\Sigma = 6 * 10^{-18} F$, $G = 2.96 * 10^{-6}\ S$, and calculate a quality factor of $Q = 1.3 * 10^6$.

REFERENCES

1. Island, J. O.; Tayari, V.; Yiğen, S.; McRae, A. C.; Champagne, A. R., *Applied Physics Letters* **2011,** 99, 243106.
2. Mariani, E.; von Oppen, F., *Physical Review B* **2009**, 80, 155411.
3. Wang, L., Ph.D. Thesis, Auburn University, **2007**.
4. Sapmaz, S.; Blanter, Y. M.; Gurevich, L.; van der Zant, H. S. J., *Physical Review B* **2003**, *67*, 235414.
5. Biercuk, M.J.; Ilani, S.; Marcus, C. M.; McEuen, P. L., *Carbon Nanotubes* **2008,** 111, 455–493.
6. Lassagne, B.; Tarakanov, Y.; Kinaret, J.; Garcia-Sanchez, D.; Bachtold, A., *Science* **2009,** 325, 1107-1110.